J. Fluid Mech. (1995), *vol.* 297, *pp.* 49–76

On the two-way interaction in two-dimensional particle-laden flows: the accumulation of particles and flow modification

By O. A. DRUZHININ

Applied Physics Institute, Russian Academy of Sciences, 603600 Nizhni Novgorod, Russia

(Received 12 September 1994 and in revised form 20 March 1995)

The evolution of two-dimensional regular flows laden with solid heavy particles is studied analytically and numerically. The particulate phase is assumed to be dilute enough to neglect the effects of particle–particle interactions. Flows with large Reynolds and Froude numbers are considered, when effects related to viscous dissipation and gravity are negligible. A Cauchy problem is solved for an initially uniform distribution of particles with Stokes (St) and Reynolds (Re_p) numbers of order unity in several types of flows representing steady solutions of the two-dimensional Euler equations. We consider flows in the vicinity of the hyperbolic stagnation point (with a uniform strain and zero vorticity) and the elliptic stagnation point (where vorticity is uniform), a circular vortex (with vorticity depending on the radius) and Stuart vortex flow. Analytical solutions are obtained, for the case of sufficiently small St, describing the accumulation of particles and corresponding modification of the fluid flow. Solutions derived show that the concentration of particles, although remaining uniform, decreases at the elliptic stagnation point and grows at the hyperbolic point. Owing to the coupling between the particulate and fluid dynamics, the flow vorticity is reduced at the elliptic point, while flow strain rate is enhanced at the hyperbolic point. Solutions obtained for the circular vortex show that the accumulation of particles proceeds in the form of a travelling wave. The concentration grows locally, forming the crest of the wave which propagates away from the vortex centre. Owing to the influence of the particulate on the carrier flow, the vorticity is reduced in the vortex centre. At the location of the crest the gradient of the flow grows owing to the drag forces between the fluid and particles and a vorticity peak is generated. Analytical solutions are also obtained for a chain of particle-laden Stuart vortices. Owing to the coupling effects, the concentration is diminished and the vorticity is reduced at the centres of the vortices. A sheet of increased concentration and vorticity is formed extending from the braid region to the periphery of the vortices, and the flow strain in the braid region is enhanced. Results of numerical simulations performed for $St = 0.5$ show good agreement with analytical solutions.

1. Introduction

Problems connected with the prediction of the evolution of fluid flows laden with solid heavy particles arise in many areas of applied and fundamental research. The dynamics of such flows is governed by a set of coupled equations describing motion of the carrier flow and the particulate phase (Soo 1967; Elghobashi & Abou-Arab 1983; Nigmatulin 1987; Shraiber *et al.* 1988). The interaction between the fluid and particles is due to the friction (or drag) forces which stem from the local slip velocity as particles

deviate from the fluid trajectories owing to the inertia. If the concentration of particles is large enough, particle–particle interactions and the exclusion of one phase by another also affect the flow dynamics. In the dilute limit the latter effects are usually negligible compared to those caused by the drag forces, unless the particles are small enough to be regarded as nearly passive tracers.

The local accumulation of heavy particles is revealed to be a common feature of the dynamics of particle-laden flows. Numerous results reported for the case when the influence of particles on the fluid flow is neglected show that local values of the particulate concentration may increase considerably. Under the influence of inertia particles drift from the regions of high flow vorticity towards the regions of high strain rate and low vorticity. This inertial bias (Maxey 1990; Wang & Maxey 1993) brings about the formation of certain patterns in the particle distribution.

Numerical studies of particle dispersion in turbulent flows show that particles accumulate at the edges of local vortex structures forming elongated sheets (Chung & Troutt 1988; Squires & Eaton 1991; Longmire & Eaton 1992; Lazaro & Lasheras 1992*a*, *b*; Tang *et al.* 1992; Wang & Maxey 1993; Martin & Meiburg 1994). The accumulation processes and pattern formation are found to be most efficient when the particle Stokes number, defined as the ratio of a characteristic time of particle motion and a flow timescale, is close to a critical value which varies depending on the flow structure and typically is of order unity. Numerical results obtained by Squires & Eaton (1991) for the particle concentration dynamics in forced homogeneous turbulence show that, owing to the inertial bias, the concentration drops in eddy zones (corresponding to vortex centres where curvature of the flow streamlines is large, the vorticity is high and the flow strain is weak) and increases considerably in convergence zones (i.e. in the vicinity of the hyperbolic stagnation points, where the flow strain rate is substantial and vorticity is low). Thus, locally, the influence of the particulate on the fluid flow may become significant and the coupling effects should be taken into account even for initially small particulate mass loading.

Numerical studies of particle dispersion in decaying isotropic turbulence performed recently by Elghobashi & Truesdell (1993) show that the two-way interaction between the two phases results in a higher dissipation rate of the fluid motions due to the increased energy of turbulence at high wavenumbers. Experimental results obtained recently by Schreck & Kleis (1993) for the particle dispersion in a grid-generated turbulence also indicate that, owing to the influence of the particles on the carrier flow, the energy cascade towards higher wavenumber components of the turbulence spectrum is enhanced and the corresponding dissipation rate is increased.

The particle dispersion processes are found to be closely related to the dynamics of organized vortex structures, which are known to be a ubiquitous feature of turbulent flows (see e.g. Crow, Gore & Troutt 1985; Wang & Maxey 1993). Thus, knowledge of the evolution of particle-laden regular flows is of importance for understanding the mechanism of coupling between the dynamics of particles and turbulence modification.

The problem of pattern formation in a particle-laden circular vortex with the coupling effects taken into account has been addressed recently for the case of small particle Reynolds (Re_p) and Stokes (St) numbers (Druzhinin 1994). Analytical solutions obtained show that the accumulation of particles proceeds in the form of a travelling concentration wave. A steep peak in the concentration develops, forming the crest of the wave which propagates away from the vortex centre. The corresponding modification of the carrier flow for this case $St \ll 1$ is found to be caused mainly by the exclusion of the fluid by the particles, which generates a radial component of the fluid velocity directed towards the vortex centre. Owing to the increased concentration of

particles, the drag force is modified by the hydrodynamical interactions between the particles and the backflow effects (Batchelor 1972), so that the growth of the concentration wave crest is reduced. Solutions obtained also show that the generation of the concentration waves occurs most efficiently for values of St close to a critical value which is found to be of order unity.

The objective of this work is to study both analytically and numerically the processes of two-way interaction in two-dimensional regular flows laden with solid heavy particles. The flow Reynolds and Froude numbers are assumed to be large enough that the viscous dissipation and the effects related to gravity are insignificant. We assume also that the particulate concentration is small enough to neglect the effects of particle–particle interactions and consider particles with Stokes number of order unity, when the accumulation processes are intense. Only the case of particles with Reynolds number of order unity is studied, when the nonlinear effects in the drag force upon the particle remain weak.

First, we study the problem analytically, deriving an approximate solution for the particle velocity in the form of a series in St. Using this solution we simplify the original set of equations and obtain analytical solutions of a Cauchy problem for an initially uniform distribution of particles in several types of flows representing steady solutions to the two-dimensional Euler equations. We consider flows in the vicinity of a hyperbolic stagnation point (where the vorticity is zero and strain rate is uniform) and of an elliptic stagnation point (where strain is weak and vorticity is uniform), and a circular vortex (where vorticity is a decreasing function of the radius).

Solutions obtained for the flow in the vicinity of the stagnation points show that the concentration decreases at the elliptic point and grows at the hyperbolic point. Owing the effects of coupling between the fluid and particle motion, the vorticity is reduced at the elliptic point, while flow strain rate is enhanced at the hyperbolic point. In this case both the particle concentration and the flow vorticity and strain fields remain uniform.

The solution for the concentration dynamics in a circular vortex is qualitatively similar to the earlier results derived for $St \ll 1$ (Druzhinin 1994). The accumulation of particles proceeds in the form of a travelling wave, when the concentration of particles increases locally forming the wave crest propagating away from the vortex centre. The process is found to be less robust for larger mass loading ratio (which is equal to the particulate volume fraction multiplied by the ratio of the particle and fluid densities). The solutions derived show that owing to the increased inertia (larger St) the particles effectively change the fluid flow, reducing vorticity in the core. At the location of the concentration maximum the flow gradient grows owing to the enhanced drag force between the two phases and a peak of the vorticity field is generated. Results obtained for $St = 0.5$ in numerical simulations are found to agree well with analytical solutions.

We also perform numerical simulations for the more complicated case of a particle-laden chain of Stuart vortices and compare numerical results with analytical solutions obtained for local flow zones (at the centres of the vortices and in the braid region, in the vicinity of the hyperbolic stagnation point between the vortices). The concentration decreases in the vicinity of the vortex centres and grows in the braid region and at the periphery of the vortices. The coupling effects result in a vorticity reduction in the vortex centres and a strain rate enhancement in the braid region of the flow. Owing to the flow advection and the accumulation process a sheet of increased concentration is formed which extends from the braid region to the periphery of the vortices (a feature revealed earlier both experimentally and numerically in a number of free shear flows seeded with heavy particles, see e.g. Chung & Troutt 1988; Longmire & Eaton 1992;

Lazaro & Lasheras 1992*a*, *b*; Tang *et al.* 1992; Martin & Meiburg 1994). At the location of the concentration maximum the drag force is enhanced, so that a sheet of increased vorticity is generated by the coupling between the fluid and particle motions. Analytical solutions for the vorticity and strain in the vicinity of the centres of the vortices and in the braid region and an estimate for the vorticity local peak at the periphery of the vortices well agree with the numerical data.

The paper is organized as follows. In §2 equations of motion describing evolution of the particulate and fluid phases in the dilute limit are formulated. Using an approximate solution for the particle velocity, the problem further is studied analytically in §3 for an initially uniform distribution of particles in flows in the vicinity of the elliptic and hyperbolic stagnation points and in a circular vortex. Results of numerical simulations performed for the circular vortex and analysis of the two-way interaction in the particle-laden Stuart flow are presented in §4. A short summary and conclusions are given in §5.

2. Governing equations

We use the equations of motion developed for dilute particle-laden flows where particle–particle collisions are negligible (Soo 1967; Elghobashi & Abou-Arab 1983; Nigmatulin 1987; Shraiber *et al.* 1988). It is assumed that particles are solid spheres of diameter d, which is much smaller than the characteristic flow lengthscale L. On a scale much greater than d but much smaller than L the particles are regarded as a continuum with volume fraction $c(r,t) = \pi d^3 n/6$, where n is the number of particles per unit volume. Further we denote as c the particle concentration (for d a uniform constant, the actual concentration n is directly proportional to c).

The conservation equations for the fluid momentum and mass are

$$(1-c)\frac{\mathrm{D}\boldsymbol{U}}{\mathrm{D}t} = -\frac{1}{\rho_f}\boldsymbol{\nabla}p - c\delta\boldsymbol{F} + (1-c)\boldsymbol{g} + \boldsymbol{\nabla}\cdot\hat{\boldsymbol{\tau}}, \tag{1}$$

$$\frac{\partial c}{\partial t} - \boldsymbol{\nabla}\cdot(1-c)\,\boldsymbol{U} = 0. \tag{2}$$

The corresponding equations for the particulate phase are

$$\mathrm{d}\boldsymbol{V}/\mathrm{d}t = \boldsymbol{F} + \boldsymbol{g}, \tag{3}$$

$$\partial c/\partial t + \boldsymbol{\nabla}\cdot c\boldsymbol{V} = 0. \tag{4}$$

The notation used in (1)–(4) is that $\boldsymbol{U}$ and $\boldsymbol{V}$ are the fluid and particle velocities, respectively, c the particulate volume fraction (or concentration), $\delta = \rho_p/\rho_f$ the ratio of the particle and fluid densities, $\boldsymbol{F}$ the force acting on the particle from the ambient fluid and $\boldsymbol{g} = -g\boldsymbol{e}_z$, $\boldsymbol{e}_z = (0,0,1)$ the acceleration due to gravity. Derivatives $\mathrm{D}/\mathrm{D}t = \partial/\partial t + \boldsymbol{U}\cdot\boldsymbol{\nabla}$ and $\mathrm{d}/\mathrm{d}t = \partial/\partial t + \boldsymbol{V}\cdot\boldsymbol{\nabla}$ are taken along the Lagrangian (fluid) path and the particle trajectory, respectively, and the notation for the viscous term is

$$(\boldsymbol{\nabla}\cdot\hat{\boldsymbol{\tau}})_i \equiv \frac{\partial}{\partial x_j}\left\{\nu(1-c)\left(\frac{\partial U_i}{\partial x_j} + \frac{\partial U_j}{\partial x_i}\right)\right\},$$

where ν is fluid kinematic viscosity.

In the case of small heavy particles (such that $d \ll L$ and $\delta \gg 1$) the main contribution to the force $\boldsymbol{F}$ is from the viscous drag, while inertial forces (due to the pressure gradient and added mass) and the Basset history force are negligible (Maxey

& Riley 1983). For particles with Reynolds number of order unity the force is described by the empirical formula (Clift, Grace & Weber 1978)

$$F = \frac{1}{\tau_p}(U - V) f(Re_p), \tag{5}$$

with parameters

$$\tau_p = \frac{d^2}{18\nu}\delta, \quad Re_p = \frac{|V-U|\,d}{\nu},$$

corresponding to the particle response time and Reynolds number, respectively, and the function $f(Re_p)$ having the form

$$f(Re_p) = 1 + 0.15 Re_p^{2/3}. \tag{6}$$

Introducing dimensionless variables

$$r' = \frac{r}{L}, \quad t' = \frac{U_0 t}{L}, \quad U' = \frac{U}{U_0}, \quad V' = \frac{V}{U_0}, \quad p' = \frac{p}{\rho_f U_0^2}, \tag{7}$$

where U_0 and L are a characteristic flow velocity and spatial scale, we can rewrite equations (1)–(4) in the form

$$(1-c)\frac{\mathrm{D}U'}{\mathrm{D}t'} = -\nabla p' + \frac{c\delta}{St}(V' - U') f(Re_p) - (1-c)\frac{\boldsymbol{e}_z}{Fr} + \frac{1}{Re_f}\nabla\cdot\hat{\boldsymbol{\tau}}', \tag{8}$$

$$\nabla\cdot[cV' + (1-c)\,U'] = 0, \tag{9}$$

$$\frac{\mathrm{d}V'}{\mathrm{d}t'} = \frac{1}{St}(U' - V') f(Re_p) - \frac{1}{Fr}\boldsymbol{e}_z, \tag{10}$$

$$\frac{\partial c}{\partial t'} + \nabla\cdot cV' = 0. \tag{11}$$

In (8)–(11) the particle Stokes number St is defined as the ratio of particle response time to a characteristic timescale L/U_0 of the flow,

$$St = \frac{\tau_p U_0}{L} = \frac{d^2\delta}{18\nu}\frac{U_0}{L}, \tag{12}$$

and parameters

$$Re_f = U_0 L/\nu, \quad Fr = U_0^2/(gL) \tag{13}$$

correspond to the flow Reynolds and Froude numbers.

The exchange of momentum between the fluid and particles is due to the drag (or friction) force and depends on the local values of both the slip velocity $V-U$ and the mass loading ratio $c\delta$. Generally, there is no 'preferred' direction of momentum exchange, i.e. particles may locally both enhance and weaken the carrier flow. The modified continuity condition (9) reflects the fact that the two phases are mutually exclusive.

In the general case the set of equations (8)–(11) can be studied numerically. However, if the particle Stokes number is sufficiently small, some useful analytical solutions can be derived. In this case the velocity of the particle adjusts to the local fluid velocity under the action of the drag force on a timescale less than the flow variation time L/U_0 (Manton 1974; Nielsen 1984; Maxey 1990; Tio *et al.* 1993*b*). Thus, using St as an expansion parameter, we can represent V in the form (Druzhinin & Ostrovsky 1994; Druzhinin 1994)

$$V = V^{(0)} + St\,V^{(1)} + St^2\,V^{(2)} + \ldots. \tag{14}$$

Here and below, for convenience, primes on the dimensionless variables are omitted. Substituting (14) into (10) and solving iteratively, we obtain solutions for zeroth-, first- and second-order terms:

$$V^{(0)} = U - e_z W_t, \tag{15}$$

$$V^{(1)} = -\frac{1}{f(Re_t)}\left(\frac{DU}{Dt} - W_t \frac{\partial}{\partial z} U\right), \tag{16}$$

$$V^{(2)} = -\frac{1}{f(Re_t)}\left(\frac{D}{Dt} V^{(1)} + (V^{(1)} \cdot \nabla) U - W_t \frac{\partial}{\partial z} V^{(1)} - \tfrac{2}{3}[f(Re_t) - 1]\frac{(V^{(1)} \cdot e_z) e_z}{W_t}\right), \tag{17}$$

where the function $f(Re)$ is given by (6). The term in (15) corresponds to the usual passive advection solution $V = U$ modified by gravitational settling with terminal velocity W_t defined from the equation

$$W_t f(Re_t) = St/Fr, \tag{18}$$

where

$$Re_t \equiv W_t d/\nu$$

is the particle Reynolds number based on W_t. When $Re_t \ll 1$ ($f(Re_t) \approx 1$), W_t obtained from (18) corresponds to the well-known result

$$W_t = St/Fr,$$

or, in dimensional form, $W_t = \tau_p g$ which equals to the Stokes terminal velocity. It follows from (16)–(18) that the nonlinearity of the drag force upon the particle reduces both the terminal velocity and inertial corrections in comparison with the linear Stokes drag law (see Wang & Maxey 1993 and references therein).

The first-order inertial correction (16) becomes dominant compared to the second-order term in (17) for sufficiently small particles, such that $St \ll 1$ (cf. Maxey 1990). Then, substituting solutions (14), (15) and (16) for the velocity into (8) and (11) we derive the following equations for the fluid flow and concentration (Druzhinin 1994):

$$(1 + c\delta)\frac{DU}{Dt} = -\nabla p + W_t c\delta \frac{\partial U}{\partial z} - (1 + c\delta)\frac{e_z}{Fr} + \frac{1}{Re_f}\nabla \cdot \hat{\tau}, \tag{19}$$

$$\nabla \cdot [cV + (1 - c)U] = 0, \tag{20}$$

$$\frac{Dc}{Dt} - W_t \frac{\partial c}{\partial z} = St\, \nabla \cdot c \frac{DU}{Dt}. \tag{21}$$

According to (19), particles with very small Stokes number effectively change the local fluid density, which can be written as $1 + c\delta$.

In the limit of negligible mass loading ratio, $c\delta \to 0$, the influence of the particular on the fluid phase can be neglected. In this case, particle dynamics and the evolution of the concentration are driven by the fluid flow. For initially uniform distribution of particles $c(r, t = 0) = c_0$ the 'source' on the right-hand side of (21) is

$$St\, c_0 \nabla \cdot DU/Dt = St\, c_0 (S_{ij} S_{jt} - \tfrac{1}{2}\omega_j \omega_j), \tag{22}$$

where $S_{ij} = \frac{1}{2}(\partial U_i/\partial x_j + \partial U_j/\partial x_i)$ and $\omega_i = \epsilon_{ijk}\, \partial U_k/\partial x_j$ are the strain rate tensor and vorticity of the flow, respectively.

It follows from (22) that the concentration decreases in regions of high vorticity and low strain rate and grows in regions of strong irrotational strain. Thus, the distribution of particles may become quite non-uniform as, owing to the inertial bias, the particles accumulate locally in corresponding flow zones (Maxey 1990; Squires & Eaton 1991;

Wang & Maxey 1993). As has been found previously, local values of the concentration may be substantial. Thus, the local mass loading ratio may become large enough for the particles to effectively influence the fluid flow, when the two-way interaction between the two phases plays an important role, even for initially small particulate concentrations. One can also expect that eddy zones of the flow with high vorticity (in the vicinity of vortex centres or elliptic stagnation points) and convergence zones of high strain (which correspond to hyperbolic stagnation points) may be affected by the particles most significantly.

As was mentioned above, some analytical and numerical results have been obtained recently for a particle-laden circular vortex for the case $St \ll 1$ (Druzhinin 1994). Now we address the problem of the two-way interaction for several types of particle-laden flows, where the eddy and convergence zones are pronounced, and consider particles with $St \leqslant 1$ when the processes of particle accumulation are intense.

We assume that the flow is regular and of a sufficiently high Reynolds number, so that viscous stresses can be omitted in (8). The case of a sufficiently small c is considered, such that both fluid continuity and viscosity are not affected by the concentration. Then, we can omit terms proportional to c in (8) and (9) (note, however, that the corresponding mass loading ratio $c\delta$ may not be small for sufficiently large δ). We assume also that the flow Froude number (13) is large (and thus W_t is small and $f(Re_t) \approx 1$) and consider the two-dimensional case, when the vertical settling does not affect the dynamics of the system, so that terms related to gravity can be neglected. Thus (8)–(11) can be rewritten in the form

$$\frac{\mathrm{D}\boldsymbol{U}}{\mathrm{D}t} = -\nabla p + \frac{c\delta}{St}(\boldsymbol{V}-\boldsymbol{U})f(Re_p), \tag{23}$$

$$\nabla \cdot \boldsymbol{U} = 0,$$

$$\frac{\mathrm{d}\boldsymbol{V}}{\mathrm{d}t} = \frac{1}{St}(\boldsymbol{U}-\boldsymbol{V})f(Re_p), \tag{24}$$

$$\frac{\partial c}{\partial t} + \nabla \cdot c\boldsymbol{V} = 0, \tag{25}$$

with the function f and parameters Re_p and St given by (6) and (12), respectively.

Further we consider a Cauchy problem for the set of equations (23)–(25) with an initially uniform distribution of particles in several types of flows representing steady solutions of the two-dimensional Euler equations.

3. The accumulation of particles and flow modification: an analytical approach

Let us consider the case of a sufficiently small Stokes number, when solution (14)–(17) for the particle velocity can be used. Taking into account corrections up to second order in St and omitting terms related to gravity we obtain a solution for the velocity in the form

$$\boldsymbol{V} = \boldsymbol{U} - St\frac{\mathrm{D}\boldsymbol{U}}{\mathrm{D}t} + St^2\left(\frac{\mathrm{D}}{\mathrm{D}t}\frac{\mathrm{D}\boldsymbol{U}}{\mathrm{D}t} + \left(\frac{\mathrm{D}\boldsymbol{U}}{\mathrm{D}t}\cdot\nabla\right)\boldsymbol{U}\right). \tag{26}$$

Substituting (26) into (23)–(25) we obtain a reduced set of equations which then is solved analytically for several types of two-dimensional flows. We study the evolution of an initially uniform particle concentration and the corresponding modification of

the carrier flow in the vicinity of a hyperbolic stagnation point (with a uniform strain and zero vorticity) and an elliptic stagnation point (where the flow vorticity is uniform and strain is weak), and in a circular vortex (with vorticity depending on the radius).

3.1. *Hyperbolic stagnation point*

Let us consider the process of particle accumulation in the flow in the vicinity of a hyperbolic stagnation point which corresponds to the convergence zone (Squires & Eaton 1991). Solutions for the fluid velocity and particle concentration fields can be represented in the form

$$U(t) = \{-a(\tau)\,x, a(\tau)\,y\}, \quad c = c(\tau), \tag{27}$$

using the notation $\tau \equiv St\,t$. We assume that the concentration and coefficient a, being uniform constants initially, $c(0) = c_0$ and $a(0) = a_0$, change with time owing to the coupling between the fluid and particles dynamics.

The flow strain is expressed as

$$S^h_{yy}(\tau) = \partial U_y/\partial y = a(\tau), \quad S^h_{xx}(\tau) = \partial U_x/\partial x = -a(\tau). \tag{28}$$

The pressure field corresponding to (23) and (27) is given by

$$p(x, y, \tau) = -\tfrac{1}{2}a^2(1+c\delta)\,(x^2+y^2). \tag{29}$$

Performing straightforward calculations we obtain from (26) an approximate solution for the particle velocity up to second order in St in the form

$$\left.\begin{aligned} V_x &\approx -ax - St\,a^2x + St^2(\dot{a}x - 2a^3x), \\ V_y &\approx ay - St\,a^2y - St^2(\dot{a}y - 2a^3y), \end{aligned}\right\} \tag{30}$$

where the overdot corresponds to the derivative $\partial/\partial\tau$. Substituting (27)–(30) into (23) we obtain the following equations for a and c:

$$\dot{a} = 2a^3\frac{c\delta}{1+c\delta}, \quad \dot{c} = 2a^2c. \tag{31}$$

Solving (31) we derive equations which define coefficient a and concentration:

$$\frac{a(t)}{a_0} = \frac{1+c\delta}{1+c_0\delta}, \quad \left(\ln\frac{c\delta}{1+c\delta} + \frac{1}{1+c\delta}\right)\Bigg|_0^t = \frac{2a_0^2}{(1+c_0\delta)^2}St\,t. \tag{32}$$

Thus for the strain we obtain

$$\frac{S^h_{xx}(t)}{S^h_{xx}(0)} = \frac{S^h_{yy}(t)}{S^h_{yy}(0)} = \frac{1+c\delta}{1+c_0\delta}. \tag{33}$$

In the case of small mass loading ratio $c\delta \ll 1$ we find from (32) and (33) that

$$c \approx c_0\exp(2a_0^2\,St\,t), \quad \frac{S^h_{xx}(t)}{S^h_{xx}(0)} = \frac{S^h_{yy}(t)}{S^h_{yy}(0)} \approx 1 + \delta(c - c_0). \tag{34}$$

Therefore, particles accumulate in the vicinity of the hyperbolic stagnation point, enhancing the local flow strain, so that both c and S grow exponentially. Physically, (34) shows that momentum is transferred from the particles to the fluid owing to the convergent structure of the flow.

We should point out that in deriving the set of equations (31) and solutions (32) we assume that particles initially move with a velocity corresponding to (26). Thus, we do

not consider a transient, after which (26) sets in, which is of the order $\Delta t \approx St$. During this initial time interval a different dynamics of the strain and vorticity fields may be found.

Note that the problem of particle motion in flow, (27), was considered earlier by Martin & Meiburg (1994), where the drag on the particle was assumed to be linear and the influence of the particulate on the fluid flow was neglected. Numerical and analytical solutions obtained show that for large St ($St \geqslant 1/4a$) motion of the particle becomes non-monotonic, such that the particle oscillates around the y-axis in the vicinity of the stagnation point. A scaling argument was proposed suggesting that the build-up of particles at the stagnation point is most robust for $St \leqslant 1/4a$, when the particle still moves along the flow streamlines without oscillations. In this study we consider St to be sufficiently small that the approximate solution (26) remains applicable.

3.2. *Elliptic stagnation point*

Let us now consider an initially uniform distribution of particles in the flow in the vicinity of an elliptic stagnation point, where the fluid velocity field is that of an elliptical 'solid' vortex (Lamb 1975). Then, solutions for the fluid velocity and concentration can be written in the form

$$\boldsymbol{U}(t) = \{-a(\tau)\, y, b(\tau)\, x\}, \quad c = c(\tau), \quad \tau \equiv St\, t, \tag{35}$$

with initial conditions

$$c(0) = c_0, \quad a(0) = a_0, \quad b(0) = b_0,$$

where product $a_0 b_0$ is a positive constant. The corresponding vorticity, strain and pressure fields are then given by

$$\left.\begin{aligned} \omega_e(\tau) = a(\tau) + b(\tau), \quad S^e_{xy} = \frac{1}{2}\left(\frac{\partial U_y}{\partial x} + \frac{\partial U_x}{\partial y}\right) = \tfrac{1}{2}[b(\tau) - a(\tau)], \\ p(x, y, \tau) = \tfrac{1}{2} ab(1 + c\delta)(x^2 + y^2). \end{aligned}\right\} \tag{36}$$

An approximate solution for the particle velocity derived from (26) for the fluid velocity $\boldsymbol{U}$ given by (35) is

$$\left.\begin{aligned} V_x &\approx -ay + St\, abx + St^2(\dot{a}y + 2a^2 by), \\ V_y &\approx ax + St\, aby - St^2(\dot{b}x + 2ab^2 x), \end{aligned}\right\} \tag{37}$$

where, as above, the overdot denotes the derivative with respect to τ. Substituting (35)–(37) into (23) we derive the following system:

$$\dot{a} = -2a^2 b \frac{c\delta}{1 + c\delta}, \quad \dot{b} = -2ab^2 \frac{c\delta}{1 + c\delta}, \quad \dot{c} = -2abc. \tag{38}$$

From (38) we find the equations from which the concentration and coefficients a and b (cf. (32)) are obtained:

$$\frac{a(t)}{a_0} = \frac{b(t)}{b_0} = \frac{1 + c(t)\,\delta}{1 + c_0\,\delta}, \quad \left(\ln \frac{c\delta}{1 + c\delta} + \frac{1}{1 + c\delta}\right)\Bigg|_0^t = -\frac{2a_0 b_0}{(1 + c_0\,\delta)^2} St\, t. \tag{39}$$

Thus, the flow vorticity and strain are given by

$$\frac{\omega_e(t)}{\omega_e(0)} = \frac{S^e_{xy}(t)}{S^e_{xy}(0)} = \frac{1 + c(t)\,\delta}{1 + c_0\,\delta}. \tag{40}$$

From (39) follows that for times $t \gg St^{-1}$ concentration decreases exponentially,

$$c(t) \sim \exp\left(-\frac{2a_0 b_0}{(1+c_0\delta)^2} St\, t\right).$$

At sufficiently large times c becomes exponentially small. Then, from (40) we derive asymptotic expressions for vorticity and strain:

$$\frac{\omega_e(t)}{\omega_e(0)} = \frac{S^e_{xy}(t)}{S^e_{xy}(0)} \approx \frac{1}{1+c_0\delta}, \quad t \gg St^{-1}. \tag{41}$$

Therefore, owing to the interaction between the two phases the particle concentration decreases exponentially, while both vorticity and strain of the flow are reduced as

$$\frac{\omega_e(t)-\omega_e(0)}{\omega_e(0)} = \frac{S^e_{xy}(t)-S^e_{xy}(0)}{S^e_{xy}(0)} \approx -\frac{c_0\delta}{1+c_0\delta} \quad \text{for} \quad t \gg St^{-1}. \tag{42}$$

Solutions (39)–(41) show that momentum is transferred from the fluid to the particles and the flow is weakened.

In the axisymmetrical case $a_0 = b_0$ flow (35), (36) corresponds to that in the 'solid' circular vortex with vorticity $\omega_e(\tau) = 2a(\tau)$. In cylindrical coordinates fluid velocity field (35) is written as

$$U_\phi = ar, \quad U_r = 0,$$

and solution (37) for the particle velocity takes the form

$$\left.\begin{aligned} V_r &= St\, U_\phi^2/r, \\ V_\phi &= U_\phi(1-2St^2a^2) - St^2 \dot{a} r = U_\phi\left\{1-\frac{2St^2a^2}{1+c\delta}\right\}. \end{aligned}\right\} \tag{43}$$

Solutions (43) for the velocity describe rotation and radial drift of the particles, so that the concentration decreases in the vortex centre (cf. Maxey 1990). Owing to the inertia, locally the particle angular velocity is less than that of the fluid, so that the momentum is 'absorbed' by the particulate under the action of the drag force while the rotation of the fluid is slowed down and vorticity is reduced.

In the above examples both particulate concentration and flow vorticity fields remain uniform. Below we consider a particle-laden circular vortex where the accumulation of particles and flow modification proceed in the form of a travelling wave.

3.3. *Concentration waves and flow modification in a circular vortex*

Let us consider an initially uniform distribution of particles in a circular vortex with angular velocity $U_\phi(r, St, t)$. Up to second order in St the solution for the particle velocity (26) in this case can be written as (cf. Druzhinin 1994 and (43))

$$\left.\begin{aligned} V_r &= St\, U_\phi^2/r, \\ V_\phi &= U_\phi\{1-2(St\, U_\phi/r)^2\} - St\,\partial U_\phi/\partial t. \end{aligned}\right\} \tag{44}$$

Substitution of (44) into (23) gives the following equations describing the evolution of the concentration and fluid angular velocity:

$$\frac{\partial c}{\partial t} + \frac{St}{r}\frac{\partial}{\partial r}(cU_\phi^2) = 0, \tag{45}$$

$$\frac{\partial U_\phi}{\partial t} + 2St\frac{U_\phi^3}{r^2}\frac{c\delta}{1+c\delta} = 0. \tag{46}$$

From the continuity condition (24), which in the axisymmetrical case is written as

$$\frac{1}{r}\frac{\partial}{\partial r} r U_r = 0,$$

we find that radial component of the fluid velocity is identically zero. The pressure in the vortex is expressed as

$$(1 + c\delta)\, U_\phi^2 / r = \partial p / \partial r. \tag{47}$$

Together with initial conditions

$$U_\phi(r, 0) = U_\phi^{(0)}(r), \quad c(r, 0) = c_0 \tag{48}$$

equations (45)–(47) represent a Cauchy problem for the two-phase flow considered here.

In the case of very small concentration, such that mass loading ratio is negligible,

$$c\delta \to 0,$$

the fluid flow remains unchanged and the particle dynamics and evolution of the concentration are driven by the fluid velocity field. Then, solution of the Cauchy problem for the concentration can be obtained after integration of (45) along characteristics in the general form (cf. Druzhinin 1994)

$$c(r, t) = c_0(r_0)\, U_\phi^2(r_0) / U_\phi^2(r), \tag{49}$$

where $U_\phi(r) = U_\phi^{(0)}(r)$ and function $r_0(r, t)$ is implicitly defined by the equation

$$\int_{r_0}^{r} \frac{r\,\mathrm{d}r}{U_\phi^2(r)} = St\, t. \tag{50}$$

As an example, we consider a steady circular flow with angular velocity field

$$U_\phi = \frac{r}{2(1 + r^2)}. \tag{51}$$

The corresponding vorticity field is then given by

$$\omega = \frac{1}{r}\frac{\partial}{\partial r} r U_\phi = \frac{1}{(1 + r^2)^2}. \tag{52}$$

Fluid flow (51) coincides with that in a 'solid' vortex with uniform vorticity $\omega_0 = 1$ for which $U_\phi \approx r/2$ for small radius ($r \ll 1$) and with that in a point vortex $U_\phi \approx 1/2r$ for $r \gg 1$. Region $r \leqslant 1$ can be regarded as the core of the vortex.

For U_ϕ defined by (51), integration of (50) can be performed explicitly. Thus, the following equation for r_0 is obtained:

$$\ln r_0 + r_0^2 + \tfrac{1}{4} r_0^4 = \ln r + r^2 + \tfrac{1}{4} r^4 - \tfrac{1}{4} St\, t. \tag{53}$$

Once function $r_0(r, t)$ is found from (53), the solution for the concentration is obtained from (49) and (51) in the form

$$c(r, t) = c_0 \left(\frac{r_0}{r}\right)^2 \left(\frac{1 + r^2}{1 + r_0^2}\right)^2. \tag{54}$$

As has been shown recently (Druzhinin 1994), solutions (53) and (54) describe a radial travelling concentration wave starting from an initially uniform particle concentration field and propagating away from the vortex centre.

Indeed, as follows from (54), at a given point r the concentration grows for $r_0(r,t) > 1$ and drops for $r_0(r,t) < 1$. Thus, as follows from (53), in the vortex core, for $r < 1$, the concentration only decreases with time, while in the outside region, for $r > 1$, it grows for $t < t_m$ (where $r_0(r, t_m) = 1$) and then decreases. The location of the concentration maximum $r = r_{cr}$ at time moment $t = t_{cr}$ is defined by the condition

$$r_0(r,t) \approx 1$$

obtained from $\partial c/\partial r = 0$ with the use of (53) for $r_{cr} \gg 1$. Thus, the locations of the wave crest $r_{cr}(t_{cr})$ and concentration maximum $c_{cr}(r_{cr}, t_{cr})$ at the crest are derived from (53) and (54) in the form

$$\ln r_{cr} + r_{cr}^2 + \tfrac{1}{4} r_{cr}^4 = \tfrac{1}{4} St\, t_{cr} + \tfrac{5}{4}, \tag{55}$$

$$c_{cr}(r_{cr}, t_{cr}) = c_0 \left(\frac{1 + r_{cr}^2}{2 r_{cr}} \right)^2. \tag{56}$$

The effective local propagation velocity $S_{cr} = \mathrm{d}r_{cr}/\mathrm{d}t_{cr}$ of the wave crest is expressed using (55) as

$$S_{cr} = \tfrac{1}{4} St \left(\frac{1}{r_{cr}} + 2 r_{cr} + r_{cr}^3 \right)^{-1}. \tag{57}$$

In the region close to the vortex centre, $r_0(r,t)$ decreases exponentially, and from (53) and (54) we find

$$r_0(r,t) \approx r \exp(-\tfrac{1}{4} St, t), \quad c(r,t) \approx c_0 \exp(-\tfrac{1}{2} St\, t) \quad \text{for} \quad r \ll 1. \tag{58}$$

For $r < r_{cr}$ at times $t \gg t_{cr}$ solutions for r_0 and c coincide with (58). In the region far away from the crest, at time $t \ll t_{cr}$, from (53) and (54) we obtain solutions for r_0 and c in the form

$$r_0^4(r,t) \approx r^4 - St\, t, \quad c(r,t) \approx c_0 r^2 (r^4 - St\, t)^{-1/2} \quad \text{for} \quad r \gg r_{cr}. \tag{59}$$

Solutions (56)–(59) describe the process of particle accumulation in the limit $c\delta \to 0$ which proceeds in the form of a travelling concentration wave. The crest of the wave propagates out of the vortex, so that the concentration grows in front of the crest, for $r > r_{cr}$, $t < t_{cr}$, and decreases exponentially for $r < r_{cr}$, $t > t_{cr}$, so that a steep well forms behind the crest (cf. Druzhinin 1994).

Let us now take into account the effects of coupling between the particles and the carrier flow.

In the vicinity of the vortex centre, flow (51) is the same as that in a 'solid' circular vortex with uniform vorticity equal to unity. Thus, solutions for the concentration and fluid flow are analogous to those obtained above for the flow in the vicinity of an elliptic stagnation point with coefficients $a_0 = b_0 = \frac{1}{2}$ (cf. (43)). Thus, we derive the following equation for the particle concentration (cf. (39)):

$$\left(\ln \frac{c\delta}{1 + c\delta} + \frac{1}{1 + c\delta} \right) \Bigg|_0^t = -\frac{St\, t}{2(1 + c_0 \delta)^2}, \tag{60}$$

while the vorticity is found from the equation (cf. (40))

$$\frac{\omega(r,t)}{\omega(r,0)} = \frac{1 + c(r,t)\,\delta}{1 + c_0 \delta}, \quad r \ll 1. \tag{61}$$

For $t \gg St^{-1}$ the concentration decreases exponentially, so that vorticity in the core is reduced as

$$\frac{\omega(r,t)-\omega(r,0)}{\omega(r,0)} \approx -\frac{c_0\delta}{1+c_0\delta} \quad \text{for} \quad t \gg St^{-1}, \quad r \ll 1, \tag{62}$$

where $\omega(0,0) = 1$.

Approximate solutions describing the dynamics of the concentration wave crest and the fluid flow modification outside the vortex core can be obtained for sufficiently small particulate mass loading ratio,

$$c\delta \ll 1.$$

A first-order correction to the dynamics of the concentration wave crest can be calculated with the use of an equation obtained from (45) and (46) in the form

$$\frac{\mathrm{d}}{\mathrm{d}t}(cU_\phi^2) = -4St\,\delta\left(c\frac{U_\phi^2}{r}\right)^2, \tag{63}$$

where derivative $\mathrm{d}/\mathrm{d}t$ is taken along characteristics,

$$\frac{\mathrm{d}r}{\mathrm{d}t} = St\frac{U_\phi^2}{r}. \tag{64}$$

Then, integrating in (63) over time we find

$$(cU_\phi^2)^{-1}|_0^t = 4St\,\delta\int_0^t \frac{\mathrm{d}t}{r^2}, \tag{65}$$

where $r(t)$ is defined by (64). Performing the integration in (65) along the 'undisturbed' crest trajectory (55), where the relation

$$St\,\mathrm{d}t = 4\left(\frac{1}{r}+2r+r^3\right)\mathrm{d}r$$

holds and using expression (51) for the velocity U_ϕ, we obtain the following expression for the concentration at the crest:

$$c_{cr} \approx c_{cr}^{(0)}\{1-\tfrac{1}{4}c_0\delta(2r_{cr}^2+8\ln r_{cr}-1-r_{cr}^{-4})\}, \tag{66}$$

where $c_{cr}^{(0)}(r_{cr})$ is given by (56). According to (66), the growth of the concentration at the crest is slowed down by the coupling for larger mass loading compared to the case $c\delta \to 0$.

The fluid velocity can be represented as a sum of the background field and a first-order correction,

$$U_\phi = U_\phi^{(0)}(r) + U_\phi^{(1)}(r,t), \tag{67}$$

where $U_\phi^{(1)}$ is described by the equation obtained from (46) to first order in $c\delta$:

$$\frac{\partial U_\phi^{(1)}}{\partial t} + 2St\,rc^{(0)}\delta\left(\frac{U_\phi^{(0)}}{r}\right)^3 = 0. \tag{68}$$

Integrating in (68) over time we derive the following solution for the velocity:

$$U_\phi(r,t) = U_\phi^{(0)}(r)\left\{1-2St\,\delta\left(\frac{U_\phi^{(0)}}{r}\right)^2\int_0^t c^{(0)}(r,t')\,\mathrm{d}t'\right\}, \tag{69}$$

where $c^{(0)}(r, t)$ is given by (54). From (69) it follows that the fluid velocity decreases as the concentration wave crest propagates away from the vortex centre. Since the concentration sharply increases for $r \approx r_{cr}$ and becomes exponentially small behind the crest, for $r < r_{cr}$, $t > t_{cr}$, a sharp gradient in the velocity field forms. The corresponding peak of the vorticity field at the location of the crest can be estimated as follows.

From (69) we obtain the following expression for the vorticity:

$$\omega = \omega(r, 0) + \Delta\omega(r, t),$$

where correction $\Delta\omega$, described by the equation

$$\Delta\omega \approx -2St \frac{\delta}{r}\frac{\partial}{\partial r}\left\{\frac{(U_\phi^{(0)})^3}{r}\int_0^t c^{(0)}(r, t')\,dt'\right\}, \tag{70}$$

is of first order in $c\delta$. Performing the integration in (70) along the crest trajectory (55) and using solution (56) for the concentration and (51) for the fluid velocity at the crest for $r_{cr} \gg 1$ we obtain an estimate for the vorticity peak at the location of the concentration wave crest in the form

$$\Delta\omega_{cr} \approx \tfrac{1}{6} c_0 \delta \quad \text{for} \quad r_{cr} \gg 1. \tag{71}$$

Therefore, solutions (60), (61), (66) and (69) describe the particle accumulation and the flow modification in the form of a travelling wave. The concentration grows locally forming the crest of the wave which propagates away from the vortex centre. Since owing to the inertia the particle angular velocity locally is less than the fluid velocity (cf. (43)), the momentum is transferred to the particulate, while the fluid angular velocity is decreased under the action of the drag force. In the vortex centre the concentration remains almost uniform and decreases exponentially and the vorticity is reduced (cf. (60), (61)). When the concentration wave crest is located sufficiently far away from the vortex core, the gradient of the fluid velocity grows owing to the enhanced drag force and the peak of the vorticity field (71) is generated at the location of the concentration wave crest.

4. Numerical results

In this section we present results of a numerical simulation of the set of equations (23)–(25) performed for the particle-laden circular vortex. We also study the processes of the two-way interaction in a chain of particle-laden Stuart vortices through numerical integration of the problem and using the analytical approach discussed above.

4.1. *Numerical simulations of the particle-laden circular vortex*

In the axisymmetrical case the set of equations (23)–(25) can be rewritten in cylindrical coordinates as

$$\frac{\partial U_\phi}{\partial t} = \frac{c\delta}{St}(V_\phi - U_\phi) f(Re_p), \tag{72a}$$

$$\frac{\partial}{\partial t}(cV_r) + \frac{\partial}{\partial r}(cV_r^2) + c\frac{V_r^2 - V_\phi^2}{r} = -\frac{c}{St} V_r f(Re_p), \tag{72b}$$

$$\frac{\partial}{\partial t}(cV_\phi) + \frac{\partial}{\partial r}(cV_r V_\phi) + 2c\frac{V_r V_\phi}{r} = \frac{c}{St}(U_\phi - V_\phi) f(Re_p), \tag{72c}$$

$$\frac{\partial c}{\partial t} + \frac{1}{r}\frac{\partial}{\partial r}(rcV_r) = 0, \tag{72d}$$

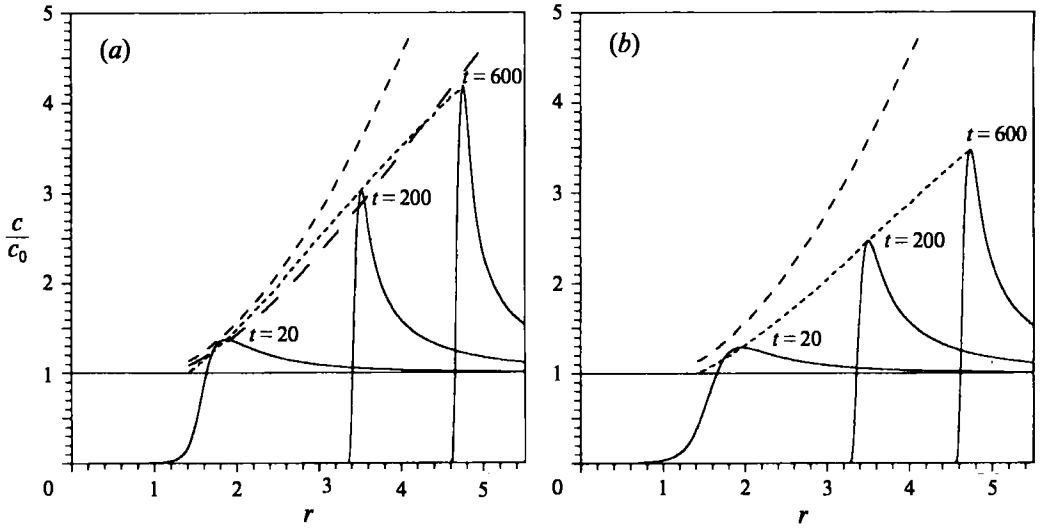

FIGURE 1. The particle concentration in the circular vortex at different times (full curves) obtained by DNS of equations (72) with an initially uniform distribution of particles in flow (73) for (*a*) $c_0\delta = 0.03$ and (*b*) $c_0\delta = 0.3$, with $St = 0.5$. Dashed and long-dashed curves correspond to solutions for the location of the crest (56) and (66), respectively. Short-dashed curves correspond to the crest trajectory obtained numerically. Here and below the dimensionless time is expressed in St^{-1} units.

where $f(Re_p)$ is given by (6). In (72) we take into account that the radial component of the fluid velocity vanishes owing to the continuity condition.

Initial conditions corresponding to a uniform distribution of particles in the circular vortex considered above are written as

$$U_\phi(r,0) = \frac{r}{2(1+r^2)} \tag{73}$$

for the fluid velocity and

$$V_\phi(r,0) = U_\phi(r,0),\ V_r(r,0) = 0, \quad c(r,0) = c_0 \tag{74}$$

for the particular velocity and concentration fields.

We used a MacCormack marching algorithm (Fletcher 1990) (see the Appendix) to solve problem (72)–(74) numerically for parameters $U_0 d/\nu = 1$, $St = 0.5$ and for two different values of the initial mass loading ratio $c_0\delta = 0.03$ (case *a*) and $c_0\delta = 0.3$ (case *b*). It was observed that in this case Re_p remained of order unity throughout the simulations.

The development of the concentration wave and the corresponding modification of the carrier flow at different times are shown in figures 1(*a*)–3(*a*) and 1(*b*)–3(*b*) for cases (*a*) and (*b*), respectively.

Solution (66) for the crest trajectory obtained for $c\delta \ll 1$ (long-dashed curve in figure 1*a*) quite accurately describes the trajectory of the crest, obtained numerically for $c_0\delta = 0.03$ (short-dashed curve in figure 1*a*). The growth of the crest is slowed down compared to the value of $c^{(0)}$ given by solution (56) derived in the limit of negligible mass loading ratio $c_0\delta \to 0$ (dashed curve in figure 1*a*) (some differences are caused by the finite value of St which is comparable to unity here). For larger values of the mass loading ratio ($c_0\delta = 0.3$ for case *b*) the growth of the concentration wave crest becomes less robust.

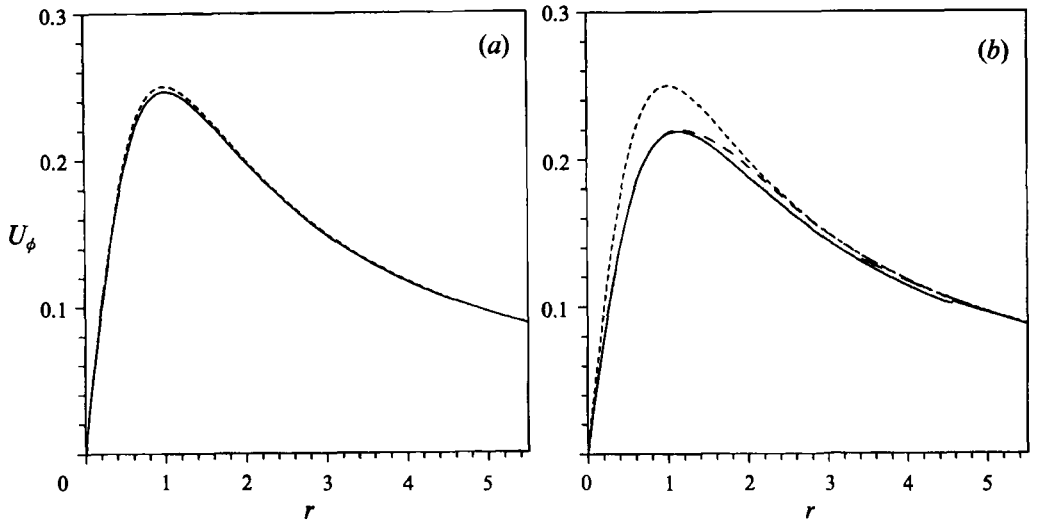

FIGURE 2. Angular fluid velocity corresponding to figure 1 (*a*, *b*) at times (*a*) $t = 0$, 600 (short-dashed and solid curves, respectively); (*b*) $t = 0$, 20, 200, 600 (short-dashed, dashed, long-dashed and solid curves, respectively).

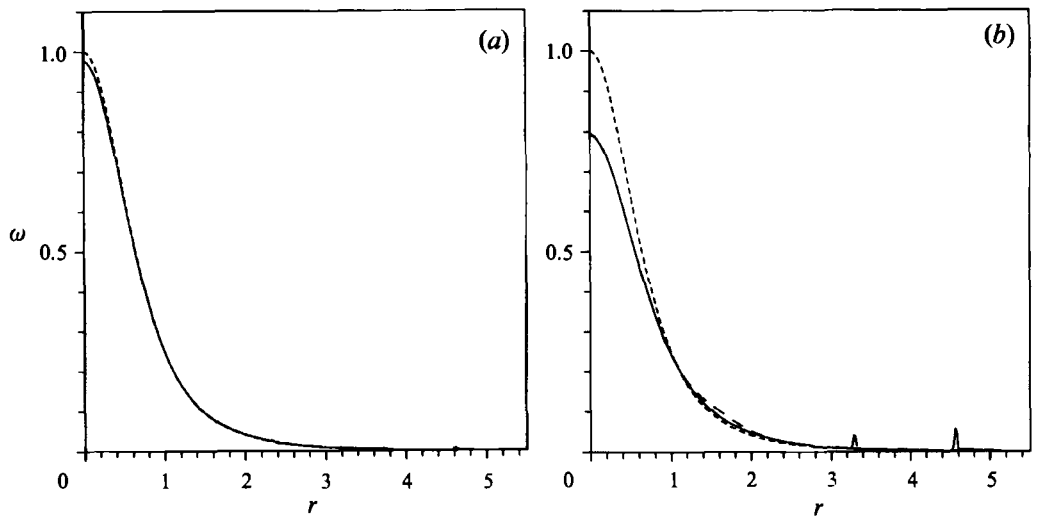

FIGURE 3. Vorticity field corresponding to figure 1 (*a*, *b*) at times (*a*) $t = 0$, 600 (short-dashed and solid curves, respectively); (*b*) $t = 0$, 20, 200, 600 (short-dashed, dashed, long-dashed and solid curves, respectively).

Numerical data for the fluid angular velocity and vorticity fields presented in figures 2(*a*, *b*) and 3(*a*, *b*) also are in good agreement with the analytical solutions. The reduction in the angular velocity and vorticity in the core of the vortex is fairly well predicted by (62) (in cases (*a*) and (*b*) we find $\omega(t) \approx 0.97$ and $\omega(t) \approx 0.73$, respectively, which are quite close to the numerical data, figures 3*a* and 3*b*). The generation of the vorticity peak at the location of the concentration wave crest is more pronounced in case (*b*), where the vorticity increases up to the value $\Delta\omega \approx 0.06$ while from estimate (71) we obtain $\Delta\omega_{cr} \approx 0.05$.

4.2. *Accumulation of particles and flow modification in a chain of Stuart vortices*

In the examples discussed above we consider flows with a simple structure. In this subsection we study the evolution of particle-laden Stuart flow. This flow consists of a chain of co-rotating vortices and may be regarded as an idealized model with a structure similar to that of a plain mixing layer (see e.g. Tio, Gañán-Calvo & Lasheras 1993*a*; Lazaro & Lasheras 1993*a*, *b*; Gañán-Calvo & Lasheras 1991). We present results of the numerical simulations and compare them with solutions derived with the use of the analytical approach discussed in §3.

In the two-dimensional Cartesian coordinates, equations for the carrier flow (23) and (24) can be represented in the 'vorticity–stream function' variables (Fletcher 1990). Introducing the flow stream function $\Psi(x, y)$ due to the continuity condition as

$$U_x = \frac{\partial \Psi}{\partial y}, \quad U_y = -\frac{\partial \Psi}{\partial x}, \tag{75}$$

and using the relation

$$\omega = -\Delta \Psi, \tag{76}$$

we obtain an equation for the vorticity in the form

$$\frac{\partial \omega}{\partial t} + \frac{\partial}{\partial x}(\omega U_x) + \frac{\partial}{\partial y}(\omega U_y) = \frac{\delta}{St}\left\{\frac{\partial}{\partial x}[c(V_y - U_y) f(Re_p)] - \frac{\partial}{\partial y}[c(V_x - U_x) f(Re_p)]\right\}. \tag{77}$$

Equations for the particulate momentum and concentration are written as

$$\left.\begin{aligned} \frac{\partial}{\partial t}(cV_x) + \frac{\partial}{\partial x}(cV_x^2) + \frac{\partial}{\partial y}(cV_x V_y) &= \frac{c}{St}(U_x - V_x) f(Re_p), \\ \frac{\partial}{\partial t}(cV_y) + \frac{\partial}{\partial x}(cV_x V_y) + \frac{\partial}{\partial y}(cV_y^2) &= \frac{c}{St}(U_y - V_y) f(Re_p), \end{aligned}\right\} \tag{78}$$

$$\frac{\partial c}{\partial t} + \nabla \cdot cV = 0. \tag{79}$$

Let us consider an initially uniform distribution of particles in the Stuart flow. This flow represents a steady solution to the two-dimensional Euler equations and is defined by the stream function which can be written as

$$\Psi(x, y) = -U_0 \ln(\cosh y - \kappa \cos x), \tag{80}$$

with a free-stream velocity $U_0 = (1-\kappa)/(1+\kappa)$. The fluid velocity and vorticity fields according to (75) and (76) are given by

$$\left.\begin{aligned} U_x = -U_0 \frac{\sinh y}{\cosh y - \kappa \cos x}, \quad U_y = U_0 \frac{\kappa \sin x}{\cosh y - \kappa \cos x}, \\ \omega = (1-\kappa)^2 \exp(2\Psi/U_0). \end{aligned}\right\} \tag{81}$$

For $0 < \kappa < 1$ flow (81) corresponds to that in a row of co-rotating vortices with vorticity equal to unity at the vortex centres (with coordinates $x = 2\pi n$, $y = 0$, $n = 0, \pm 1 \ldots$). In the limiting case $\kappa = 0$ the flow coincides with that in the tanh-mixing layer, while for $\kappa = 1$ it corresponds to a row of point vortices. In the numerical simulations we used $\kappa = 0.5$ (the corresponding stream function (80) and vorticity field (81) are shown in figure 4*a*, *b*).

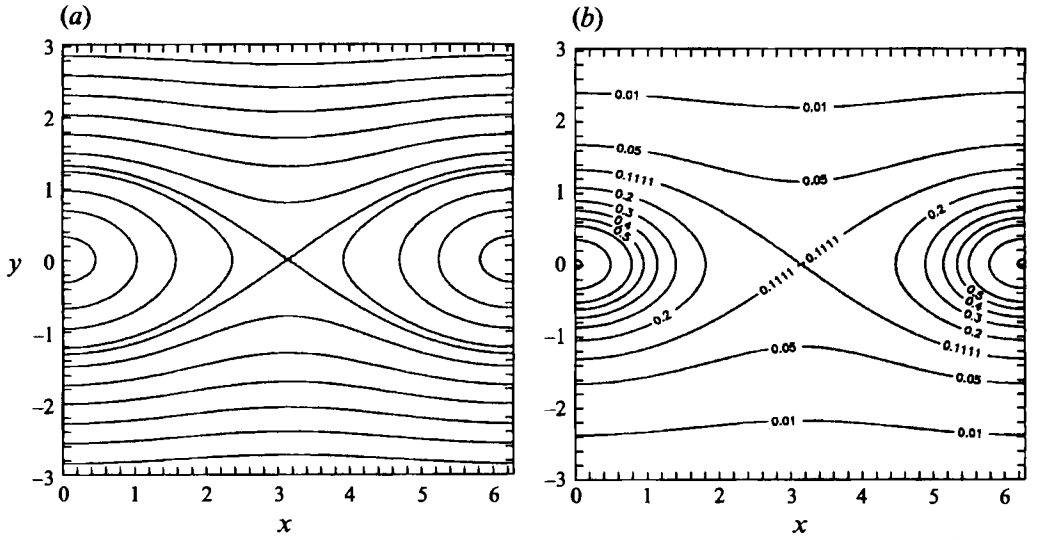

FIGURE 4. (*a*) Stream function (80) and (*b*) vorticity (81) for the Stuart vortex flow with $\kappa = 0.5$.

We solved the Poisson equation (76) defining the flow stream function for a given vorticity field and advanced equations (77)–(79) in time using a MacCormack marching algorithm (Fletcher 1990). We used a 100×100 grid in the region $0 < x < 2\pi$, $-\pi < y < \pi$ with periodic boundary conditions over x and the free-stream velocity condition $U_y = 0$, $U_x = \pm U_0$ for $y = \mp\pi$. The grid used was found to be large enough to resolve the flow scales essential for the present study. The parameter choice used was analogous to that in case (*b*) for the circular vortex ($U_0 d/\nu = 1$, $St = 0.5$, $c_0\delta = 0.3$). Initially the fluid velocity and vorticity were as given by (81) (figure 4). The particulate velocity was initially equal to the fluid velocity, the concentration being a uniform constant. As was observed for the case of the circular vortex (§4.1), for this parameter choice the particle Reynolds number also remained of order unity.

The concentration and vorticity fields at times $t = 7$ and 14 are presented in figures 5(*a*, *b*) and 6(*a*, *b*) respectively.

The concentration of particles decreases at the centres of the vortices (which correspond, in fact, to elliptic stagnation points) and increases in the braid region, in the vicinity of the hyperbolic stagnation point between the vortices (figure 5*a*, *b*). At times $t > 10$, owing to the accumulation and the flow advection processes, a sheet of increased particle concentration develops extending from the braid region to the peripheries of the vortices (figure 6*a*, *b*).

The vorticity is reduced in the vortex centres and is increased at the location of the concentration maximum. At later stages pronounced sheets of increased vorticity and concentration are formed (figures 6*a*, *b* and 7).

In order to apply the analytical approach used in §3, it is convenient to consider different zones of the flow (Squires & Eaton 1991), corresponding to the vortex centres (i.e. eddy zones in the vicinity of the elliptical stagnation points with coordinates $x = 0, 2\pi$, $y = 0$) and to the braid region (i.e. the convergence zone in the vicinity of the hyperbolic stagnation point $x = \pi$, $y = 0$).

Let us first consider the centres of the vortices $x_e = 0, 2\pi$, $y_e = 0$, where the fluid velocity field (81) can be represented locally as (cf. (35))

$$U_x \approx -a_e(t)\, y, \quad U_y \approx b_e(t)\, x \tag{82}$$

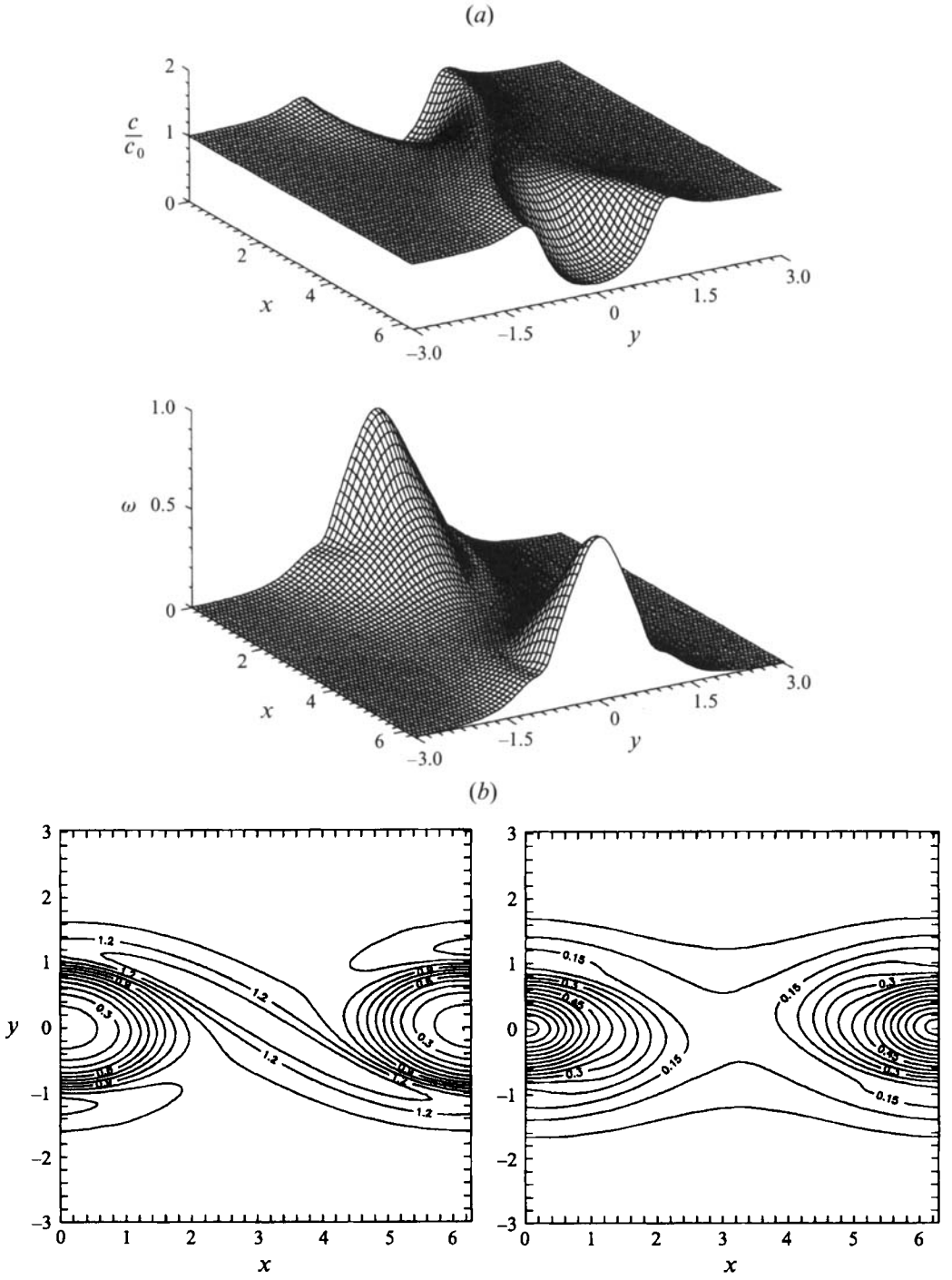

FIGURE 5. Results of DNS of the Stuart flow with an initially uniform distribution of particles. (*a*) Surfaces and (*b*) contour maps of the particulate concentration (top) fluid vorticity fields (bottom) obtained at $t = 7$ for $c_0\delta = 0.3$, $St = 0.5$.

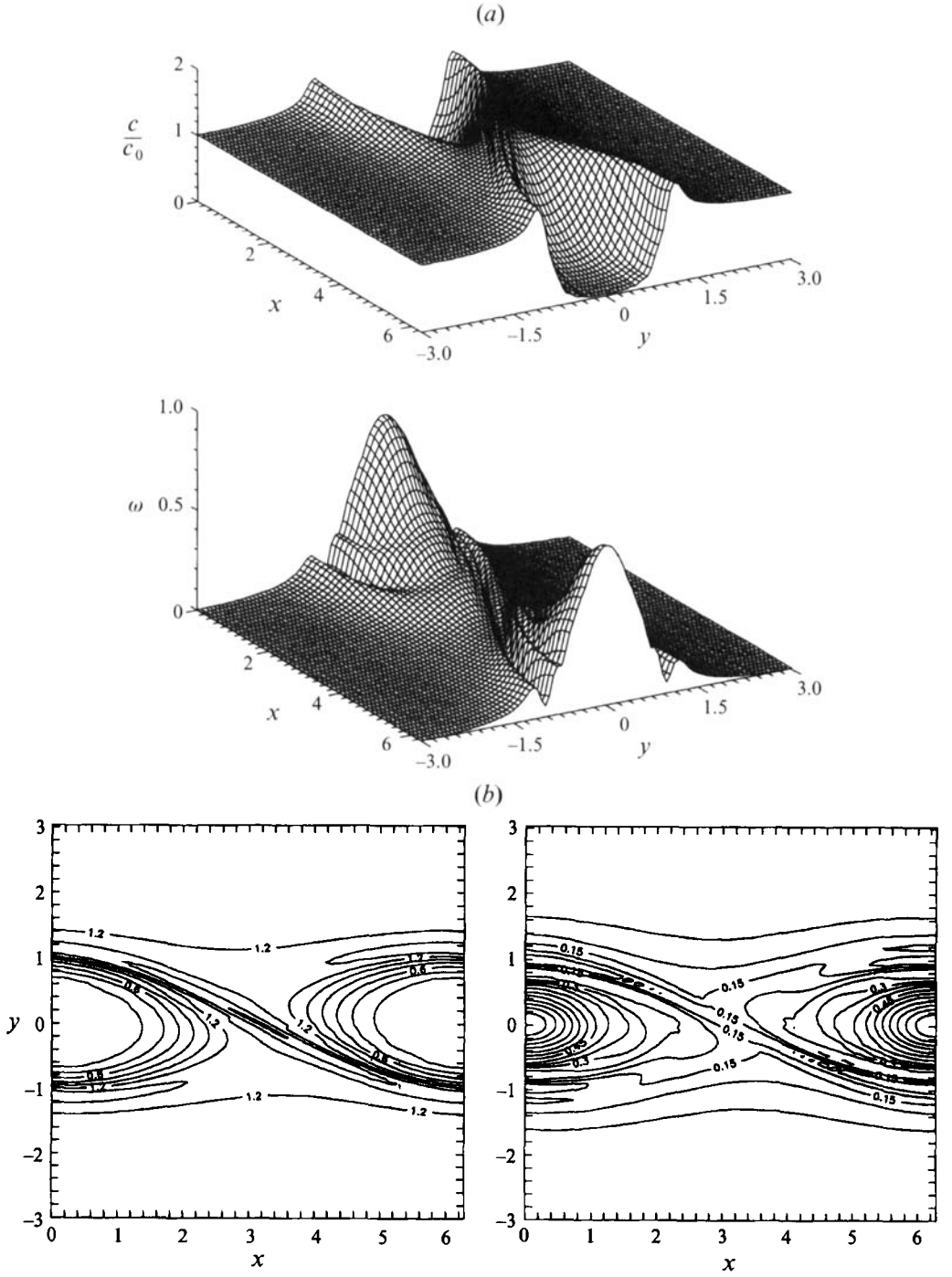

FIGURE 6. (*a*) Surfaces and (*b*) contour maps of the particulate concentration and fluid vorticity fields corresponding to figure 5(*a*, *b*) but at $t = 14$.

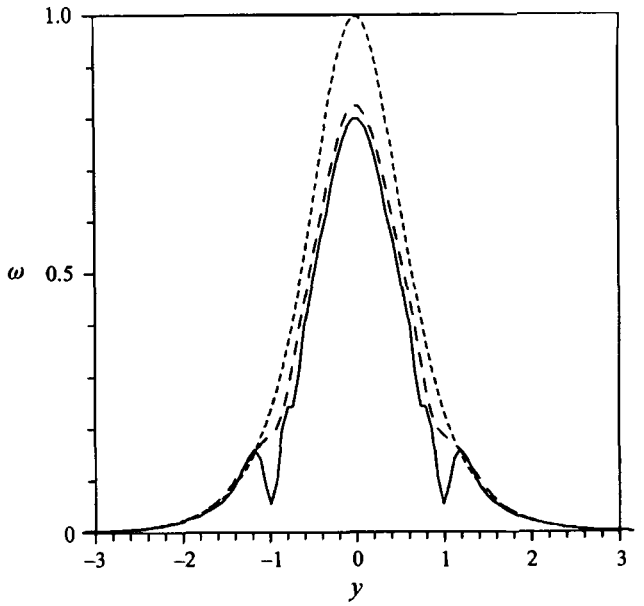

FIGURE 7. Cross-section of the vorticity surface $\omega(x = 0, y)$ at times $t = 0, 7, 14$ (short dashed, dashed and solid curves, respectively) corresponding to figures 5(*a*) and 6(*a*).

for $|x|, |y| \ll 1$. Coefficients a_e, b_e are initially equal to $a_e(0) = 1/(1+\kappa)$, $b_e(0) = a_e(0)\,\kappa$. Then, the problem of the evolution of the flow (82) with an initially uniform distribution of particles is identical to that for the elliptic stagnation point considered in §3.1. Solutions for the concentration and flow vorticity and strain are obtained in the form (cf. (39), (40))

$$\left.\begin{aligned} \left(\ln\frac{c\delta}{1+c\delta}+\frac{1}{1+c\delta}\right)\Bigg|_0^t &= -\frac{2\kappa}{(1+\kappa)^2}\frac{St\,t}{(1+c_0\,\delta)^2}, \\ \frac{S^e_{xy}(t)}{S^e_{xy}(0)} &= \frac{\omega_e(t)}{\omega_e(0)} = \frac{1+c\delta}{1+c_0\,\delta}. \end{aligned}\right\} \tag{83}$$

Therefore, for $t \gg St^{-1}$ the concentration decreases exponentially, while the vorticity is reduced as

$$\frac{\omega_e(t)-\omega_e(0)}{\omega_e(0)} \approx -\frac{c_0\,\delta}{1+c_0\,\delta}, \tag{84}$$

where $\omega_e(0) = 1$ in the case considered.

In the braid region, in the vicinity of the hyperbolic stagnation point $x_h = \pi$, $y_h = 0$ the fluid flow is locally given by

$$U_x \approx -a_h(t)\,y, \quad U_y \approx -b_h(t)\,x, \tag{85}$$

where $|x|, |y| \ll 1$, and for the coefficients we initially have $a_h(0) = U_0/(1+\kappa)$, $b_h(0) = a_h(0)\,\kappa$. Expressions for the local strain and vorticity are

$$S^h_{xy} = -\tfrac{1}{2}(a_h+b_h), \quad \omega_h = a_h-b_h. \tag{86}$$

The solutions for the particle velocity, coefficients a_h, b_h and concentration can be derived in a way analogous to that discussed in §3.2. (Note, however, that in the case

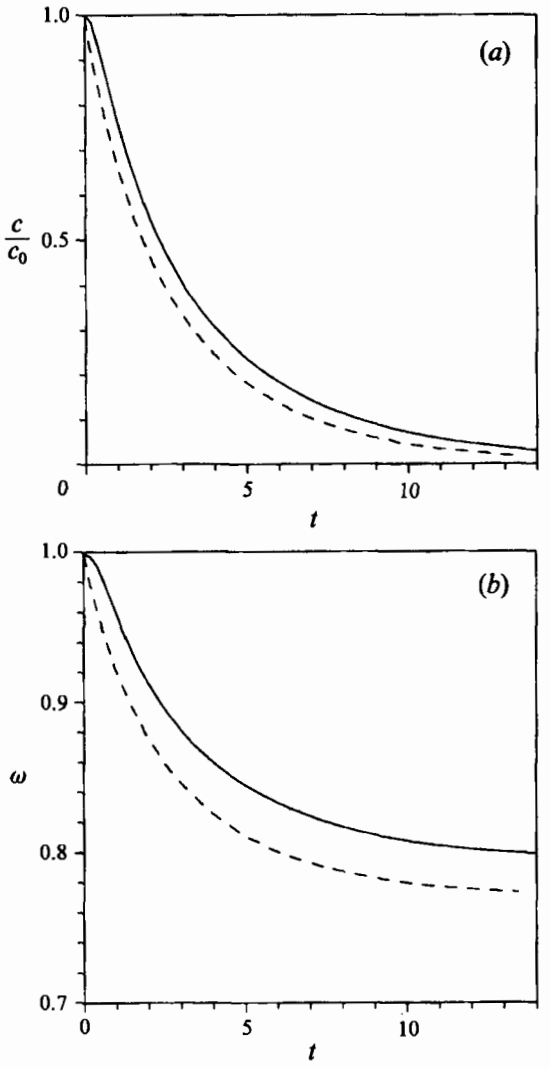

FIGURE 8. Time dependence of (*a*) the concentration and (*b*) vorticity at the vortex centre $x = 0, y = 0$ corresponding to figures 5 and 6. Numerical data are represented by solid curves, dashed curves correspond to (83).

considered here the flow is not potential.) Thus, the particulate concentration and the flow strain and vorticity are define by the equations (cf. (32))

$$\left.\begin{aligned} \left(\ln\frac{c\delta}{1+c\delta}+\frac{1}{1+c\delta}\right)\Big|_0^t &= \left(\frac{U_0}{1+\kappa}\right)^2\frac{2\kappa}{(1+c_0\delta)^2}St\,t, \\ \frac{S^h_{xy}(t)}{S^h_{xy}(0)} &= \frac{\omega_h(t)}{\omega_h(0)} = \frac{1+c(t)\delta}{1+c_0\delta}. \end{aligned}\right\} \tag{87}$$

It follows from (87) that the particle concentration and both flow vorticity and strain in the braid region grow with time.

We performed an analysis of the particle motion in the flow (85) similar to that done by Martin & Meiburg (1994) for $c_0\delta = 0$ (no influence of the particles on the fluid flow) and $f(Re_p) = 1$ (the viscous force is the linear Stokes drag force). We find that

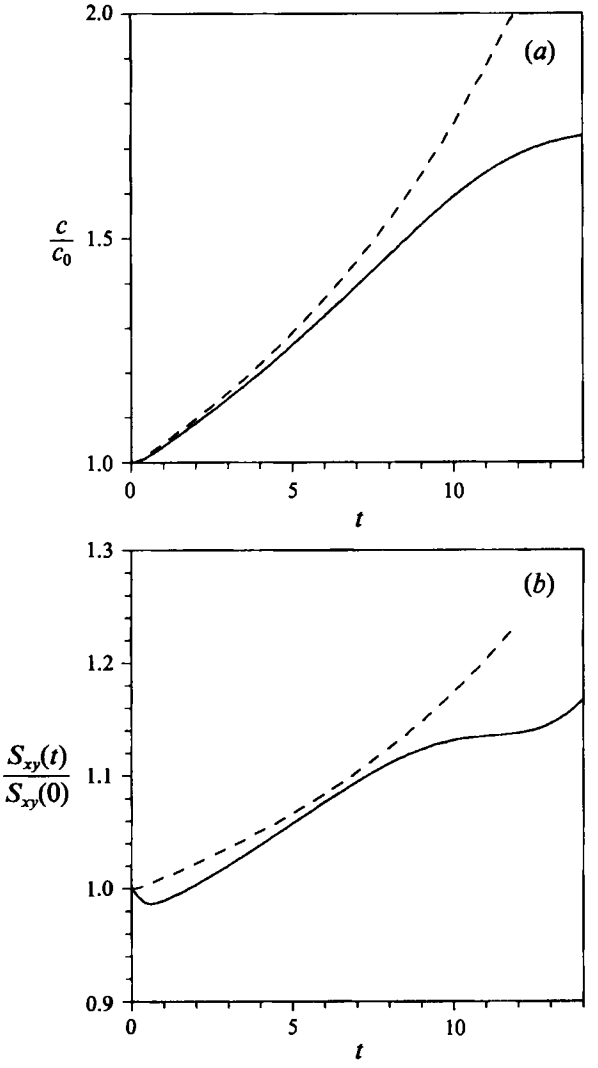

FIGURE 9. Time dependence of (*a*) the concentration and (*b*) flow strain at the hyperbolic stagnation point $x = \pi$, $y = 0$ (in the braid region). Numerical data are represented by solid curves, dashed curves correspond to (87).

oscillatory motions of the particle arise for $St > St_c = 1/[4(a_h b_h)^{1/2}]$. Thus, for the value $\kappa = 0.5$ considered here we find $St_c = 9.4\sqrt{2} \approx 1.6$. In the numerical simulations we take $St = 0.5$ which is always smaller than St_c, which ensures the applicability of solutions (87).

Solutions (83) and (87) are compared with the numerical data in figures 8 (*a*, *b*) and 9(*a*, *b*). The time dependence of the vorticity and concentration obtained numerically at the vortex centres (solid curves in figure 8 *a*, *b*) agree well with solutions (83) (dashed curves). At the hyperbolic point there is good agreement between the numerical data and solutions (87) for the local strain and concentration for times $t \leqslant 10$, when S_{xy} and c remain locally uniform (figure 9 *a*, *b*) (a slight reduction of the strain for $t \leqslant 1$ is related to the initial conditions for the particulate velocity). At later stages the concentration and flow strain and vorticity fields become strongly non-uniform (figure

6*a*, *b*). As c grows locally, the sheet of increased concentration is generated owing to the particle accumulation and flow advection processes. Owing to the drag force the flow gradient and the vorticity are increased at the location of the sheet (figures 6*a*, *b* and 7).

The value of vorticity peak $\omega_{cr}(x, y)$ at the location of the concentration maximum $c_{cr}(x, y_{cr})$ at the periphery of the vortices, for $|x| \ll 1$, $y \approx y_{cr} > 1$, can be estimated for small mass loading ratio $c\delta \ll 1$ as follows.

The vorticity can be represented as a sum

$$\omega = \omega^{(0)}(x, y) + \Delta\omega(x, y, t), \tag{88}$$

where correction $\Delta\omega$ is of first order in $c\delta$. In the region considered, the fluid flow (81) can be represented as

$$U_x \approx -U_0(1 + 2\kappa e^{-y}\cos x), \quad U_y \approx 2\kappa U_0 e^{-y}\sin x, \tag{89}$$

and solution (26) for the particle velocity is

$$\left.\begin{aligned} V_x &\approx U_x + 2St\,U_0^2\kappa e^{-y}\sin x + 2St^2\,U_0^3\kappa e^{-y}\cos x, \\ V_y &\approx U_y + 2St\,U_0^2\kappa e^{-y}\cos x - 2St^2\,U_0^3\kappa e^{-y}\sin x. \end{aligned}\right\} \tag{90}$$

Keeping only terms proportional to the derivative $\partial c/\partial y$ which is large compared to the velocity derivatives and derivative $\partial c/\partial x$ we derive from (77) an equation for the correction $\Delta\omega$ in the form

$$\frac{\partial}{\partial t}\Delta\omega \approx -\frac{\delta}{St}(V_x - U_x)\frac{\partial c}{\partial y}. \tag{91}$$

Expressing $\partial c/\partial y$ as

$$\frac{\partial c}{\partial y} \approx \frac{\partial c}{\partial t}\frac{1}{V_y},$$

substituting the expression for the velocity (90) and integrating over time in (91), we find an estimate for the local vorticity peak:

$$\Delta\omega_{cr} \approx c_{cr}\,U_0\,\delta, \tag{92}$$

where c_{cr} corresponds to the local concentration maximum.

For the parameters considered ($\kappa = 0.5$, $c_0\,\delta = 0.3$) and the value of the concentration maximum at $x = 0$, $t = 14$ obtained numerically, $c_{cr}/c_0 \approx 1.2$ (figure 6*a*, *b*), we obtain from (92) $\Delta\omega_{cr} \approx 0.12$, which is close to the numerical data (figure 7).

We did not perform computations for larger times, when smaller scales of the flow are generated which would require a higher spatial resolution. The numerical simulations were performed in order to demonstrate how the two-way interaction develops at the characteristic flow zones and to compare numerical data with analytical results. We did not study the effects of the nonlinearity in the drag force upon the particles for larger Re_p. In the case considered, $Re_p \leqslant 1$, these make the generation of the concentration waves less robust (as the nonlinearity causes a faster adjustment of the particle velocity to the local fluid velocity and reduces the effects of inertia (cf. Wang & Maxey 1993).

5. Conclusions

The processes of the two-way interaction in two-dimensional flows laden with solid heavy particles have been studied both analytically and numerically in the dilute limit (negligible particle–particle interactions). Regular flows with large Reynolds and

Froude numbers have been considered, where effects related to viscous dissipation and gravity can be disregarded as insignificant. We have considered an initially uniform distribution of particles with Stokes (St) and Reynolds (Re_p) numbers of order unity in several types of flows representing steady solutions of the two-dimensional Euler equations. In particular, flows in the vicinity of the hyperbolic stagnation point (with a uniform strain and zero vorticity) and the elliptic stagnation point (where vorticity is uniform), a circular vortex (with vorticity depending on the radius) and Stuart vortex flow have been studied.

Analytical and numerical solutions obtained describe the accumulation of particles and corresponding modification of the carrier flow. Solutions derived show that the concentration of particles decreases at the vortex centres (i.e. in eddy zones where the flow vorticity and curvature of the streamlines are high and the flow strain is weak) and grows at the periphery of the vortices and in the braid regions (in convergence zones, in the vicinity of the hyperbolic stagnation point, where the flow strain is strong and vorticity is low). The accumulation processes result in the generation of sheets of increased concentration extending from the braid region to the peripheries of the vortices. This is in agreement with previous findings and corresponds to the inertial bias effects discussed by many authors (see e.g. Maxey 1990; Squires & Eaton 1991; Wang & Maxey 1993).

Owing to the coupling between the particle and fluid dynamics, the vorticity in the centres of the vortices is reduced, while the strain rate at the hyperbolic point of the flow grows. At the locations of the concentration sheets gradients of the fluid velocity are increased because of the drag forces between the two phases and sheets of increased vorticity are formed.

The results obtained may have useful implications for the modification of turbulent flows by dispersed heavy particles. Results of DNS of particle dispersion in decaying isotropic turbulence (Elghobashi & Truesdell 1993) and experimental data for grid-generated turbulence seeded with heavy particles (Schreck & Kleis 1993) obtained recently show that the coupling between fluid and particulate dynamics leads to an enhanced energy cascade from the large-scale to small-scale components of the fluid motions and, hence, to a higher dissipation rate. Now it is well established that localized vortex structures represent an inherent feature of turbulent flows related to their intermittent nature (see e.g. She, Jackson & Orszag 1990; Ruetsch & Maxey 1991, 1992 and references therein). The dissipation rate of the local kinetic energy of the fluid motion ϵ is related to the flow strain tensor $S_{ij} = \frac{1}{2}(\partial U_i/\partial x_j + \partial U_j/x_i)$ and fluid kinematic viscosity ν as $\epsilon = 2\nu\langle S_{ij} S_{ij}\rangle$, where angular brackets denote an average over an ensemble of realizations of the turbulent flow considered (Landau & Lifshitz 1987). Thus, the effects of the vorticity reduction at the centres of the vortices, enhancement of the strain in the braid region between the vortices and generation of the vortex sheets at the location of the sheets of increased concentration, discussed in this paper for several types of regular flows, may contribute to the energy cascade towards smaller scales and cause a higher dissipation rate in particle-laden turbulent flows.

Of course, the model flows considered in this study are very simple compared to a real turbulent flow, where motions occur on a wide range of scales. On the other hand, the inertial bias effects and, hence, the pattern formation in the particulate distribution are most efficient when the timescale of the carrier flow is of the order of the particle response time (see e.g. Crow *et al.* 1985; Chung & Troutt 1988; Squires & Eaton 1991; Tang *et al.* 1992; Wang & Maxey 1993; Martin & Meiburg 1994; Druzhinin 1994). Thus, there are always 'distinguished' modes of the flow which influence the particulate most effectively. In this study we have considered idealized flow models

which may correspond to such modes and reflect some features of the two-way interaction between the particles and organized vortex structures in turbulence.

The author is grateful to the referees for valuable comments and criticism. This work was supported by the Basic Research Foundation of Russia (RFFI grant N 93-02-16166) and by Goskomvuz of Russia.

Appendix. Numerical scheme

The set of equations (72) is discretized in accordance with the MacCormack marching algorithm (Fletcher 1990) as follows.

The first (predictor) step calculates the intermediate values of U_ϕ^*, V_ϕ^*, V_r^* and c^* of the angular fluid velocity, particulate angular and radial velocities, and concentration, respectively:

$$U_{\phi j}^* = U_{\phi j}^t + \frac{\delta}{St}\Delta t\, c_j^t (V_{\phi j}^t - U_{\phi j}^t) f(Re_j^t),$$

$$P_{rj}^* = P_{rj}^t - \frac{\Delta t}{\Delta r}(Fpr_{j+1}^t - Fpr_j^t) - \frac{\Delta t}{St} P_{rj}^t f(Re_j^t) - \frac{\Delta t}{r_j}(Fpr_j^t - V_{\phi j}^t P_{\phi j}^t),$$

$$P_{\phi j}^* = P_{\phi j}^t - \frac{\Delta t}{\Delta r}(Fp\phi_{j+1}^t - Fp\phi_j^t) - 2\frac{\Delta t}{r_j} Fp\phi_j^t - \frac{\Delta t}{St} c_j^t f(Re_j^t)(V_{\phi j}^t - U_{\phi j}^t),$$

$$c_j^* = c_j^t - \frac{\Delta t}{\Delta r}(P_{rj+1}^t - P_{rj}^t) - \frac{\Delta t}{r_j} P_{rj}^t.$$

The second (corrector) step obtains the values of

$$U_\phi^{t+\Delta t},\ V_r^{t+\Delta t},\ V_\phi^{t+\Delta t},\ c^{t+\Delta t}$$

as

$$U_{\phi j}^{t+\Delta t} = 0.5\left[U_{\phi j}^t + U_{\phi j}^* + \frac{\delta}{St}\Delta t\, c_j^*(V_{\phi j}^* - U_{\phi j}^*) f(Re_j^*)\right],$$

$$P_{rj}^{t+\Delta t} = 0.5\left[P_{rj}^t + P_{rj}^* - \frac{\Delta t}{\Delta r}(Fpr_j^* - Fpr_{j-1}^*) - \frac{\Delta t}{St} P_{rj}^* f(Re_j^*) - \frac{\Delta t}{r_j}(Fpr_j^* - V_{\phi j}^* P_{\phi j}^*)\right],$$

$$P_{\phi j}^{t+\Delta t} = 0.5\left[P_{\phi j}^t + P_{\phi j}^* - \frac{\Delta t}{\Delta r}(Fp\phi_j^* - Fp\phi_{j-1}^*) - 2\frac{\Delta t}{r_j} Fp\phi_j^* - \frac{\Delta t}{St} c_j^* f(Re_j^*)(V_{\phi j}^* - U_{\phi j}^*)\right],$$

$$c_j^{t+\Delta t} = 0.5\left[c_j^* + c_j^t - \frac{\Delta t}{\Delta r}(P_{rj}^* - P_{rj-1}^*) - \frac{\Delta t}{r_j} P_{rj}^*\right].$$

The following notation is used:

$$P_r = V_r c, \quad P_\phi = V_\phi c, \quad Fpr = P_r V_r, \quad Fp\phi = P_\phi V_r,$$

and $V_{rj}^t = V_r(r = j\Delta r, t)$, $c_j^t = c(r = j\Delta r, t)$, etc. The following boundary conditions are imposed:

$$\left.\frac{\partial c}{\partial r}\right|_{r=0} = \left.\frac{\partial c}{\partial r}\right|_{r=r_{max}} = 0, \quad U_\phi = V_\phi = V_r = 0 \quad \text{at} \quad r = 0, \left.\frac{\partial V_r}{\partial r}\right|_{r=r_{max}} = 0, \quad \left.\frac{\partial V_\phi}{\partial r}\right|_{r=r_{max}} = 0.$$

The algorithm was checked for the case $c_0\delta = 0$ (no influence of the particulate on the fluid flow). The accuracy attained was found to be $O(\Delta r^2, \Delta t^2)$. In the numerical simulations we used $\Delta r = 0.02$, $\Delta t = 0.002$, $r_{max} = 10$.

In the case of the Stuart flow, equations (77)–(79) were discretized in two-dimensional Cartesian coordinates (x, y) in the domain $0 < x < 2\pi$, $-\pi < y < \pi$ in accordance with the MacCormack marching scheme similar to that above. We used the grid 100×100 and advanced the system with the time step $\Delta t = 0.01$. Solving the Poisson equation (76) we performed the Fourier transform over the x-coordinate, used the Thomas algorithm over the y-coordinate and then transformed the solution back, obtaining the value of the stream function for the given vorticity field (Fletcher 1990).

REFERENCES

BATCHELOR, G. K. 1972 Sedimentation in a dilute suspension of spheres. *J. Fluid Mech.* **52**, 245–268.

CHUNG, J. N. & TROUTT, T. R. 1988 Simulations of particle dispersion in an axisymmetric jet. *J. Fluid Mech.* **186**, 199–222.

CLIFT, H., GRACE, J. R. & WEBER, M. E. 1978 *Bubbles, Drops and Particles.* Academic.

CROW, C. T., GORE, R. & TROUTT, T. R. 1985 Particle dispersion by coherent structures in free shear flows. *Particulate Sci. Tech.* **3**, 149–158.

DRUZHININ, O. A. 1994 Concentration waves and flow modification in a particle-laden circular vortex. *Phys. Fluids* **6**, 3276–3284.

DRUZHININ, O. A. & OSTROVSKY, L. A. 1994 The influence of Basset force on particle dynamics in two-dimensional flows. *Proc. NATO ARW Chaotic Advection, Tracer Dynamics and Turbulent Dispersion (May 1993).* Physica **D76**, 34–43.

ELGHOBASHI, S. E. & ABOU-ARAB, T. W. 1983 A two-equation turbulence model for two-phase flows. *Phys. Fluids* **26**, 931.

ELGHOBASHI, S. E. & TRUESDELL, G. C. 1993 On the two-way interaction between homogeneous turbulence and dispersed solid particles. I. Turbulence modification. *Phys. Fluids* A **5**, 1790–1802.

FLETCHER, C. A. J. 1990 *Computational Techniques for Fluid Dynamics*, Vols. 1 and 2. Springer.

GAÑÁN-CALVO, A. M. & LASHERAS, J. C. 1991 The dynamics and mixing of small spherical particles in a plane free shear layer. *Phys. Fluids* A **3**, 1207–1217.

LAMB, H. 1975 *Hydrodynamics*, 7th edn. Cambridge University Press.

LANDAU, L. D. & LIFSHITZ, E. M. 1987 *Hydrodynamics.* Pergamon.

LAZARO, B. J. & LASHERAS, J. C. 1992*a* Particle dispersion in the developing free shear layer. Part 1. Unforced flow. *J. Fluid Mech.* **235**, 143–178.

LAZARO, B. J. & LASHERAS, J. C. 1992*b* Particle dispersion in the developing free shear layer. Part 2. Forced flow. *J. Fluid Mech.* **235**, 179–221.

LONGMIRE, E. K. & EATON, J. K. 1992 Structure of a particle-laden round jet. *J. Fluid Mech.* **236**, 217–257.

MANTON, M. J. 1974 On the motion of a small particle in the atmosphere. *Boundary-Layer Met.* **6**, 487–504.

MARTIN, J. E. & MEIBURG, E. 1994 The accumulation and dispersion in forced two-dimensional mixing layers. I. The fundamental and subharmonic cases. *Phys. Fluids* **6**, 1116–1132.

MAXEY, M. R. 1990 On the advection of spherical and non-spherical particles in a non-uniform flow. *Phil. Trans. R. Soc. Lond.* A **333**, 289–307.

MAXEY, M. R. & RILEY, J. J. 1983 Equation of motion for small rigid sphere in a nonuniform flow, *Phys. Fluids.* **26**, 883–889.

NIELSEN, P. 1984 On the motion of suspended sand particles. *J. Geophys. Res.* **89**, 616–626.

NIGMATULIN, R. I. 1987 *Dynamics of Multiphase Flows*, Vols. 1 and 2. Moscow: Nauka (in Russian).

RUETSCH, G. R. & MAXEY, M. R. 1991 Small-scale features of vorticity and passive scalar fields in homogeneous isotropic turbulence. *Phys. Fluids* A **3**, 1587–1597.

RUETSCH, G. R. & MAXEY, M. R. 1992 The evolution of small-scale structures in homogeneous isotropic turbulence. *Phys. Fluids* A **4**, 2747–2760.

SCHRECK, S. & KLEIS, S. 1993 Modification of grid-generated turbulence by solid particles. *J. Fluid Mech.* **249**, 665–688.

SHE, Z.-S., JACKSON, E. & ORSZAG, S. A. 1990 Intermittent vortex structures in homogeneous turbulence. *Nature* **344**, 226.

SHRAIBER, A. A., GAVIN, L. B., NAUMOV, V. A. & YATSENKO, V. P. 1988 *Turbulent Flows in Gas Suspension*. Hemisphere.

SOO, S. L. 1967 *Fluid Dynamics of Multiphase Systems*. Waltham, MA: Blaisdell.

SQUIRES, K. D. & EATON, J. K. 1991 Preferential concentration of particles by turbulence. *Phys. Fluids* A **3**, 1169–1178.

TANG, L., WEN, E., YANG, T., CROWE, C. T., CHUNG, J. N. & TROUTT, T. R. 1992 Self-organizing particle dispersion mechanism in a plane wake. *Phys. Fluids* A **4**, 2244–2251.

TIO, K.-K., GAÑÁN-CALVO, A. M. & LASHERAS, J. C. 1993*a* The dynamics of small heavy rigid spherical particles in a periodic Stuart vortex flow. *Phys. Fluids* A **5**, 1679–1693.

TIO, K.-K., LIÑÁN, A., LASHERAS, J. C. & GAÑÁN-CALVO, A. M. 1993*b* On the dynamics of buoyant and heavy particles in a periodic Stuart vortex flow. *J. Fluid Mech.* **254**, 671–699.

WANG, L.-P. & MAXEY, M. R. 1993 Settling velocity and concentration distribution of heavy particles in homogeneous isotropic turbulence. *J. Fluid Mech.* **256**, 27–68.